Topological Data Analysis for Particulate Gels

Alexander D. Smith, Gavin J. Donley, Emanuela Del Gado,* and Victor M. Zavala*

ACCESS | Metrics & More | Article Recommendations

ABSTRACT: Soft gels, formed via the self-assembly of particulate materials, exhibit intricate multiscale structures that provide them with flexibility and resilience when subjected to external stresses. This work combines particle simulations and topological data analysis (TDA) to characterize the complex multiscale structure of soft gels. Our TDA analysis focuses on the use of the Euler characteristic, which is an interpretable and computationally scalable topological descriptor that is combined with filtration operations to obtain information on the geometric (local) and topological (global) structure of soft gels. We reduce the topological information obtained with TDA using principal component analysis (PCA) and show that this provides an informative low-dimensional representation of the gel structure. We use the proposed computational framework to investigate the influence of gel preparation (e.g., quench rate, volume fraction) on soft gel structure and to explore dynamic deformations that emerge under oscillatory shear in various response regimes (linear, nonlinear, and flow). Our analysis provides evidence of the existence of hierarchical structures in soft gels, which are not easily identifiable otherwise. Moreover, our analysis reveals direct correlations between topological changes of the gel structure under deformation and mechanical phenomena distinctive of gel materials, such as stiffening and yielding. In summary, we show that TDA facilitates the mathematical representation, quantification, and analysis of soft gel structures, extending traditional network analysis methods to capture both local and global organization.

KEYWORDS: topological data analysis, soft gels, colloids, rheology, multi-scale structure, Euler characteristic
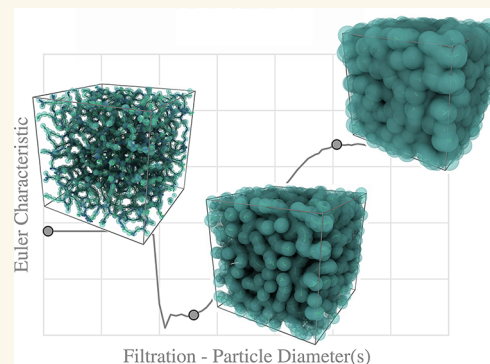
INTRODUCTION

Particulate gel technology offers a versatile solution with widespread applications across diverse industries, including pharmaceuticals, foods, and construction. In the pharmaceutical and medical device industries, these gels play a pivotal role, serving as effective drug delivery vehicles, encapsulation systems, and scaffolds. Their deformability enables the seamless incorporation of various compounds, medications, or diagnostic agents, contributing to enhanced bioavailability and therapeutic efficacy in patient care.[1−3] Within the food industry, soft gel encapsulation is employed for the delivery of functional ingredients, vitamins, and supplements. The encapsulation of sensitive compounds not only enhances their stability but also facilitates precise dosage control, meeting the growing consumer demand for convenient and palatable nutritional solutions.[4−7] In the construction sector, the utility of soft gels extends to the realm of binders, sealants, adhesives, and coatings, contributing to improved performance and durability of building materials.[8−11]

Gel formation may proceed through phase separation, aggregation, and self-assembly of polymers, colloids, or other soft matter components.[12] The stochastic and multiscale nature of these mechanisms produces hierarchical, amorphous

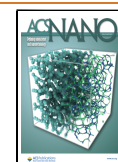structures, and provides texture, elasticity, and stability.[12−16] The multiscale structure of gels can be represented mathematically as networks defined by the interactions of their building blocks (e.g., particles, droplets, polymer aggregates). These network representations provide insight into the deformation of soft gels, and aid in understanding their mechanical failure.[12−14,17,18] For example, while soft gels can accommodate large deformations, microscale cracks that result from the accumulation of local tension can nucleate and trigger macroscopic failure, in susceptible points determined by both the local spatial distribution (geometry) and the large scale connectivity (topology) of the gel network.[12,16] It has been previously found that network structures are not static but highly dynamically reconfigurable; deformations, such as squeezing or stretching, and deformation rates can modify the mechanical characteristics of a gel by altering its network struc-

ture.[12,13,16,19−21] In addition, relaxation of the stresses accumulated in the gel through the gel formation itself, under different environmental conditions, is another important source of restructuring.[12,13,19]

The adaptable nature of particulate gel materials, their flexibility and tunability, provide exciting opportunities to precisely control and design both geometry and topology of the particle networks, potentially opening up a broad space for metamaterials design and discovery.[22−24] The geometry of the structure (its local properties) can be controlled through the physical chemistry of particles and solvent, particles surface properties, or depletion interactions,[25] and, in certain cases, is directly accessible experimentally through confocal microscopy imaging.[26−28] However, gaining access to the large-scale (global) organization of the full network and its topology remains a challenge. This limitation is important, because it is becoming increasingly clear that a hierarchical organization of the gel structure controls their mechanical response.[29] Specifically, the mechanical response of particulate gels has been observed to be nonlocal in a range of recent studies, from the emergence of rigidity to the microscopic dynamics during aging or under stress.[30,31] There is also increasing evidence of a hierarchical organization of stress transmission through the gel structure in the linear viscoelastic response.[29,32] Computer simulations can provide access to this type of information, although many of the methods used in understanding the structure of gels focus exclusively on geometry or topology, but not both. From a geometric perspective, the computation of the particle radial distribution functions provides a link to scattering experiments and constitutes an excellent tool to quantify the local structure,[33−35] but this does not capture the topology of the network.[36−38] Voronoi and Delaunay tesselation can capture properties such as cavity size distribution,[39−41] but provide limited quantification tools of the topology of a gel structure.

Graph-theoretic methods use graph descriptors (e.g., modularity, average path length, bond number, and minimal cycle basis) to quantify the structure of a network.[12,18,42] These descriptors, however, are based on averages of local topological structures and thus might fail to capture the multiscale nature of soft gels. Parametric methods based for example on distance thresholds or k-nearest neighbors commonly used to identify a graph[43] provide results which are often highly susceptible to the selection of parameter (e.g., distance threshold, k-neighbors), which is problematic if the parameter selection is not obvious from the data and rooted in the physics of the system. It is also worth noting that some of these graph-theoretic methods are computationally expensive. The computational costs become rapidly daunting for networks that are reconfigurable in nature, requiring a dynamical analysis. For example, the identification of a minimal cycle basis for a graph is at least polynomial in the number of nodes and edges present,[44] requiring significant computational time for simulations of soft gel structures from simulations which contain hundreds of thousands of nodes and edges to be able to reproduce the heterogeneities typical of real materials. It is also important to highlight that a network/graph is inherently a 2-dimensional object; as such, these representations might miss important information on the 3-dimensional structure of soft gels.

In this work, we propose an approach, based on particle simulations and topological data analysis (TDA), that captures both the geometry and topology of the 3-dimensional structure of soft particulate gels. Specifically, we focus on the application of the Euler characteristic (EC),[36,45] which is an intuitive,

interpretable, and computationally scalable topological descriptor. This approach quantifies the structure of the gel network using basic topological invariants such as the number of connected components, cycles (holes), and voids. These topological descriptors aim to quantify the structure of the gel. We use a mathematical technique known as a filtration to quantify how topological invariants emerge and disappear at different length scales. This information is condensed in a topological summary known as the EC curve. In other words, the EC curve provides a concise summary on the topological features of the gel at different length scales; this enables the detection, for instance, of hierarchical or recurrent structures. TDA approaches have been successfully applied in the analysis of complex materials, simulations, and flow networks.[36,45−51] The approaches allow us to bypass the need for parameter selection, improving the robustness of our analysis in comparison to other parametric methods (e.g., distance thresholding, neighbor selection). Moreover, these approaches allow us to capture both topological (global) and geometrical (local) characteristics of soft gel structures.[52,53]

We find that our proposed computational framework effectively represents, quantifies, and summarizes the multiscale nature of gel structures obtained from particle-based simulations. We reduce the topological information obtained with TDA using principal component analysis (PCA) and show that this provides an informative low-dimensional representation of gel structure. The application of the proposed computational framework reveals the influence of variations of the gelation kinetics on the local organization of the gels, alongside with the impact of volume fraction changes on both local and global structural aspects. The EC values clearly change with varying the degree of filtration, expressing precisely the different organization of the gel networks over different length scales, and allowing us to extract their full structural hierarchy. The analysis demonstrates that there is a direct link between the onset of gelation and the variation of the EC with filtration, as it captures the sensitivity to changes in the particle volume fraction and in the gelation protocol of the gel structures.

Furthermore, our analysis identifies topological transitions underpinning the onset of nonlinear response and flow when the gels are subjected to large amplitude oscillatory tests, clearly disentangling recoverable/unrecoverable changes from damage accumulation and revealing their hierarchical nature. We find a direct link between the exclusively structural information contained in the PCA of the Euler characteristic and the time dependent stress and strain, indicating a definite connection between the topology of the microscopic structure and the macroscopic yielding of the gels.

The methods presented here are computationally scalable (analysis of large simulations can be done in seconds-minutes and on a personal computer), interpretable, and require minimal data. The proposed approach can also be used for analysis of experimental data (such as confocal imaging), providing a route for a more direct comparison of particle simulation and experiments.[54−56] All data and scripts needed for reproducing the results are shared as open-source code.

RESULTS

To understand and quantify the structure of particulate gel simulations, we combine particle simulations with the analysis of topological invariants of the gel structures based on the EC, filtration operations, and PCA. These methods are combined to represent and quantify the gel structures across multiple length
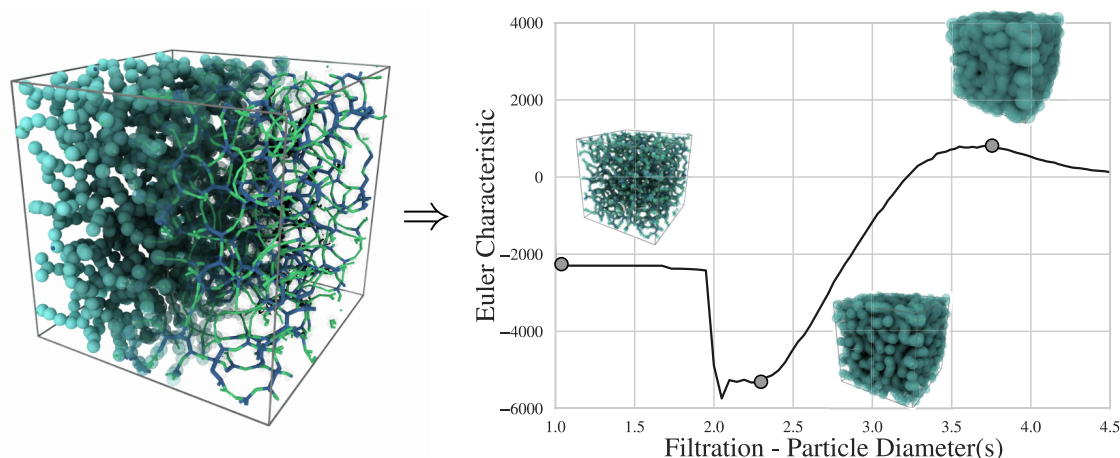
Figure 1. (Left) Visualization of a soft gel for a single simulation frame. We provide this visualization to illustrate how the various topological features: components, holes, voids, could evolve during a filtration. (Right) EC curve for the gel simulation along with a visualization of the changes in the simulation topology at various filtration diameters. The EC curve captures various topological characteristics found at multiple scales within the soft gel and show how the topological features such as holes (~2.3 particle diameters) and large voids (~3.7 particle diameters) emerge. We also note that there is minimal change in topology between $D = 1$ and $D = 2$ particle diameters. This stable topology reflects the bonded structure of the gel, and is often what is studied via network analysis tools. As we pass to $D > 2$ particle diameters, we see large topological transitions in the material, which now reflects the 3-dimensional structure of the gel and captures overlap between particles that are not necessarily directly bonded.

scales and capture the changes they undergo during shear. PCA is used to visualize topological changes and provides insight into the impact of diverse drivers on gel response (such as strain stiffening/hardening or yielding). A summary of the computational workflow to quantify the hierarchical topology of a soft gel is presented in Figure 1.

Topological Analysis of Particle Simulations. We use a particulate gel model that captures most aspects of microscopic dynamics and rheology of this class of materials. Each gel is composed of N particles, which interact via attractive short-range interactions of maximum strength ϵ, mediated by the solvent in which they are immersed and through which their thermal motion is overdamped. Surface roughness, shape irregularity and sintering processes can limit the relative motion of particles as they aggregate in real materials. These effects are included in the model through an angular modulation of the net attraction that introduces a bending rigidity of the interparticle bonds.[13,19,29,30,57] We use a cubic box of size L with periodic boundary conditions and number density N/L^3 which corresponds to an approximate solid volume fraction $\phi = \frac{N\pi d^3/6}{(Ld)^3}$. For each value of ϕ, various gel microstructures are obtained by tuning the rate Γ at which the relative strength of the attractive interactions (with respect to $k_\mathrm{B}T$) is increased to induce gelation during the sample preparation (see Methods). Finally, we subject a subset of the gels to large amplitude oscillatory shear (LAOS) deformation and extract the rheological response from the virial stress tensor (see Methods).

The numerical model used here has been shown to recapitulate a broad range of behaviors detected in experiments, in terms of structural, dynamical, mechanical, and rheological characteristics. The local particle coordination in the model gels is consistent with experimental observation in a range of colloidal systems.[26,34,54,58] The multiscale structural heterogeneities in the model gels have been shown to produce dynamical heterogeneities and microscopic relaxation consistent with experiments.[30] From these, the linear and nonlinear

mechanical responses also capture many of the experimental observations reported.[12,19,29]

The 3-dimensional gel structures obtained from particle simulation are characterized in terms of three topological invariants: the number of connected components β_0, of holes β_1, and of voids captured by β_2 (these so-called Betti numbers are combined to obtain the EC number).[36] A void is an empty cavity within a shape that is surrounded on all sides by a solid boundary. To provide an intuitive understanding of the difference between voids and holes, we can think of an open cell versus a closed cell gel or foam. An open cell structure contains many holes, whereas a closed cell structure contains many voids. To quantify the multiscale structure of our soft gel simulations we perform filtrations using increasing particle diameter and quantify the topology of the resulting Čech complex (simplicial complex) through the EC. The filtration diameter is scaled such that $D = 1$ represents the true diameter of the simulation particles. For example, a filtration radius $D = 2$ represents a Euclidean ball that is twice as wide as the original gel particle. We illustrate the filtration process on a gel simulation snapshot in Figure 1, and we also visualize the topological changes for the full simulation, which contains ~16,000 particles, as the particle diameter is increased. We do this to illustrate how the various topological invariants: components, cycles, voids, could evolve during a filtration.

Figure 1 shows how the multiscale structure of soft gels can be directly quantified through topology and filtrations. The topology of the gel goes through various topological phase transitions as the filtration diameter is increased. At $D = 1$ to $D = 2$ particle diameters we see a stable network topology. This stable topology reflects the bonded structure of the gel, and is often what is studied via network analysis tools. This network is dominated by cycles, and yields a negative Euler characteristic. As we pass to $D > 2$ particle diameters we see large topological phase transitions. Here we see a large increase in the number of cycles, an increasingly negative EC value, and the formation of an open cell structure. The measured structure now reflects the 3-dimensional structure (e.g., packing) of the gel and captures
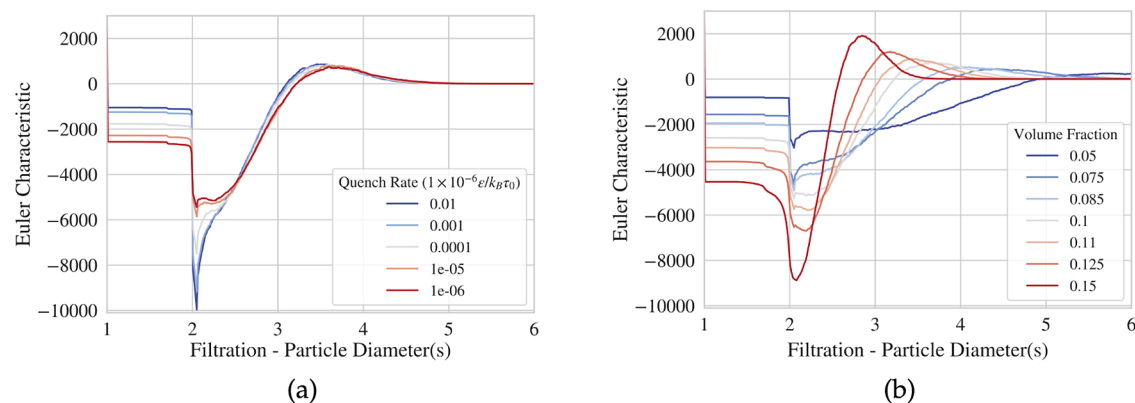
Figure 2. (a) EC curves computed from gels at various quench rates with same volume fraction (0.1). (b) EC curves computed from gels at various volume fractions and same quench rate ($1 \times 10^{-6} \, \epsilon/k_B\tau_0$, with ϵ and τ_0 respectively the unit energy and time in the simulations). There is a continuous change in the topology/geometry of the gels as quench rate and volume fraction are changed. There are significant differences in the way the larger scale structure of the gel is changed when either volume fraction or quench rate is changed. This suggests that these parameters can be used to create bespoke gel structures.

overlap between particles that are not necessarily directly bonded. Finally, at $D > 3.5$ particle diameters, we see a transition from the open cell structure dominated by cycles to the closed cell structure that is dominated by voids driving the EC to a positive value.

We leverage these topological characterizations to understand the relationship between soft gel structure and variance in the preparation parameters for the soft gel. In Figure 2 we show a direct comparison of the EC curves for soft gels with varying volume fraction (for a constant quench rate at which the gel was formed in the simulations) and for soft gels formed with varying quench rates (at a constant volume fraction of 0.10). We see that there is a smooth deformation of the EC curves with respect to changes in these two parameters, but the way in which these parameters change the gel structure is different. For the soft gels with varying quench rate shown in Figure 2a, we see that the changes in the soft gel are primarily impacting the local bonding structure ($D = 1-2.3$ particle diameters) and we see minimal changes in the larger scale structure ($D > 2.3$ particle diameters). This suggests that changing the quench rate may modify the local structure of the gel, but less so its mesoscopic 3-dimensional organization. Thus, quench rate could be used to tune/control the local organization of a soft gel without necessarily impacting its large-scale organization. In Figure 2b we see that the same is not true when volume fraction is changed; specifically, here we see that there is a large change in gel topology across multiple length scales. Interestingly, the impact on local bonding topology ($D = 1-2$ particle diameters) for increasing volume fraction follows a similar trend to decreasing quench rate, but diverges at larger scales ($D > 2$ particle diameters). This suggests that a combination of quench rate and volume fraction tune/control could be used to create soft gels with targeted structures.

Another important aspect in the application of TDA methods is computational scalability. The methods employed here are able to process gel simulations with 16,000−160,000 particles in a few minutes and on a single laptop computer. Other methods that attempt to capture similar information, such as minimal basis cycles of a graph, often run in polynomial time on the number of edges and nodes in a graph.[59] Furthermore, these graph-theoretic methods are focused at a single length scale; as such, attempting to perform these computations across various length scales would compound computational costs and affect

overall scalability. Moreover these methods represent structure as a 2-dimensional object and thus might miss important information on how the network graph is embedded in 3-dimensional space.

Gel Dynamics − Shear Analysis. The ability to rapidly quantify the topology of these gel structures allows us to perform high-throughput analysis of large temporal data sets, as those found in the analysis of gel rheology.[60,61] Here, we explore the topological and geometric deformations of soft gels as they undergo oscillatory shear. The time-averaged amplitude sweep response of the gel studied here is shown in Figure 3a. Due to the density of information contained in the time-resolved rheological responses, we restrict our analyses to three key transition amplitudes:[61] the transitions (1) between the linear and nonlinear elastic regimes, (2) the nonlinear elastic and yielding regimes, and (3) the yielding and flow regimes. These transitions occur in this specific gel system at amplitudes of 0.1, 0.35, and 1.0 strain units, respectively (see Figure 3a). At each of these amplitudes, we display time-resolved rheological and structural data extracted at a frequency of 32 points per period of oscillation.

Figure 3b illustrates the dynamic evolution of EC curves for a soft gel undergoing various amplitudes of oscillatory shear that induce linear, nonlinear, and flow regime responses. The same initialized gel is used (volume fraction: 0.10, quench rate: $1 \times 10^{-6} \, \epsilon/k_B \, \tau_0$, using the simulations reduced units) but is exposed to different shear amplitudes. This figure also shows the initial EC curve (initial topology) in the lightest color and the darkest color representing the final EC curve (final topology). We see that each simulation begins at the exact same EC curve but evolves differently as the strain amplitude is changed, though the specific changes are difficult to discern. To more clearly visualize the changes in the EC curves as the system is sheared, we used PCA to project the EC curves to a low-dimensional space (see Methods section). Figure 3c visualizes the projection of all EC curves onto the first two principal components (orthogonal dynamic modes) of the collective data set. We found that the projection onto the first two orthogonal dynamic modes accounts for approximately 98% of the variance in the EC data.

Figure 3c shows that PCA effectively captures the maximum amount of variation in the data with the minimum number of dynamic modes. This analysis reveals that there are two orthogonal dynamic behaviors captured in this low-dimensional
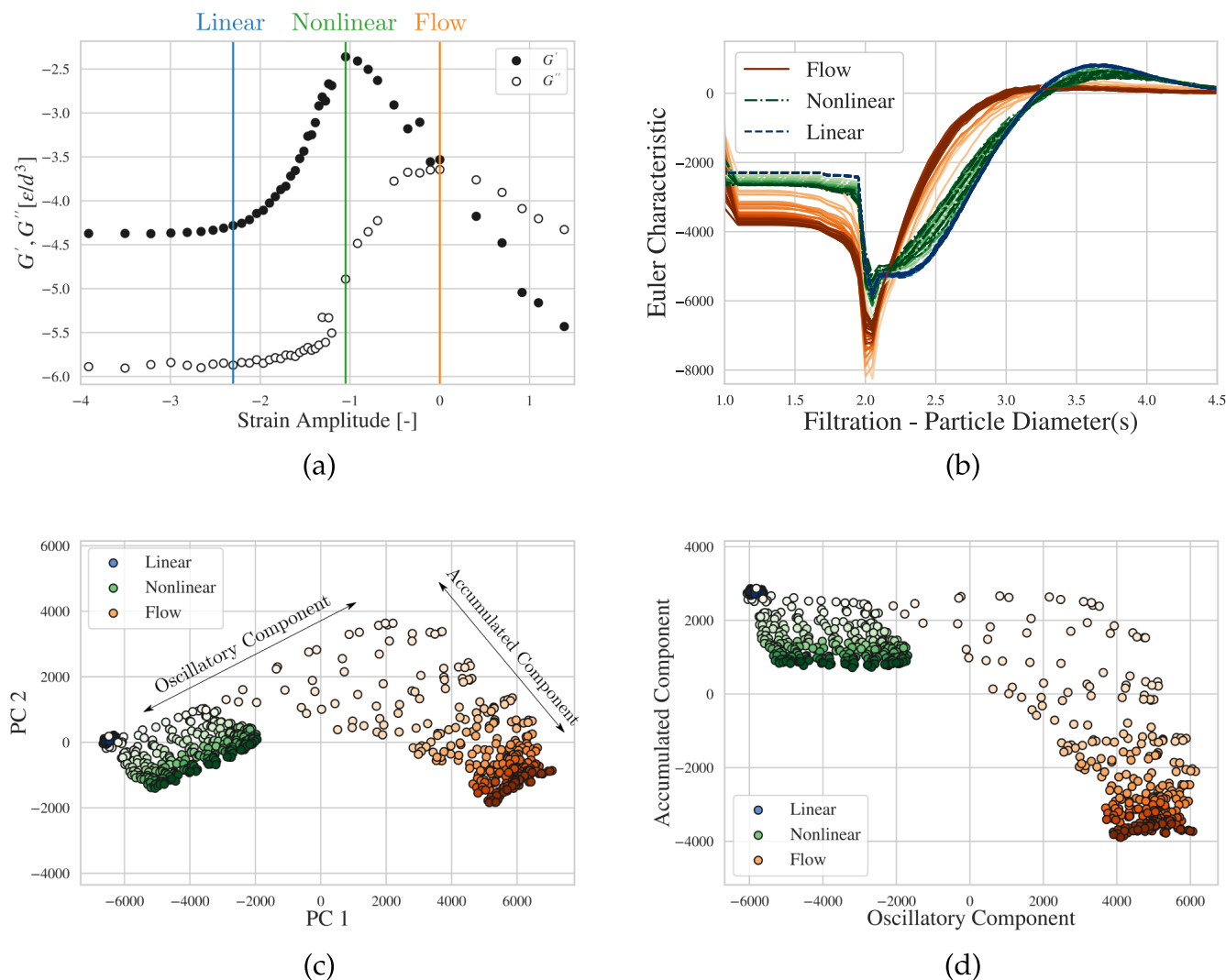
Figure 3. (a) Plot of the evolution of G' and G'' with increasing strain amplitude. The three vertical lines represent the strain amplitudes that are studied during oscillatory shear experiments. (b) EC curves computed at various temporal snapshots for a soft gel that is undergoing linear, nonlinear, and flow response to shear. The dynamic evolution is illustrated by difference in color, with the initial EC curves in the lightest color and the darkest color representing the final EC curve. We see that each simulation begins at the exact same EC curve but evolve very different as the strain amplitude is changed. (c) PCA applied to the EC curve data to create a low-dimensional representation of the dynamics of the gel during three different shear amplitudes. PCA captures 98% of the variance in the data; we see two orthogonal dynamic modes that emerge, one associated with the fast oscillations of the gel induced by oscillatory shear and a slower mode capturing cumulative structure changes. (d) Optimal rigid rotation matrix is applied to the dynamic modes so that we may observe the cumulative and oscillatory components independently.

representation: one that contains much of the fast oscillatory dynamics associated with the gel oscillation (we call this the oscillatory component) and one that contains a slow cumulative structural dynamic change within the soft gels, in particular for the nonlinear and flow regimes (we call this the accumulated/cumulative component). To directly analyze these dynamic modes in the data, we can apply a rigid rotation matrix to the first two principal component so that we may observe the cumulative and oscillatory components independently. The resulting rotated visualization is found in Figure 3d. Details around the rigid rotation and criterion for optimal rotation can be found in the Methods section.

We transformed the high-dimensional set of EC curves into a couple of simple scalar values that describe the dominating dynamic modes emerging during shearing. Figure 4a,c shows how these values evolve during the three simulations. Because PCA is a linear method, we can identify what portions of the EC

curve are associated with each dynamic mode by observing the weighting of the EC curve by the oscillatory and cumulative components shown in Figure 4b,d. Here, a larger gray area represents a higher weighting of that specific portion of the EC curve. This information reveals that the oscillatory component is capturing changes in the mesoscale structure of the soft gel ($D >$ 2.3 particle diameters) while the cumulative component is capturing local changes in the soft gel network ($D <$ 2.3 particle diameters).

Figure 4a captures much of the oscillatory behavior that is induced by the oscillatory shearing of the gel. The linear response regime shows minimal deformation and all deformation seems to be elastic as there are no continuous offsets in the data. The same is true for the nonlinear response, but we see larger oscillations which are expected as the strain amplitude has increased. The flow response shows multiple interesting characteristics that differentiate it from the linear and nonlinear
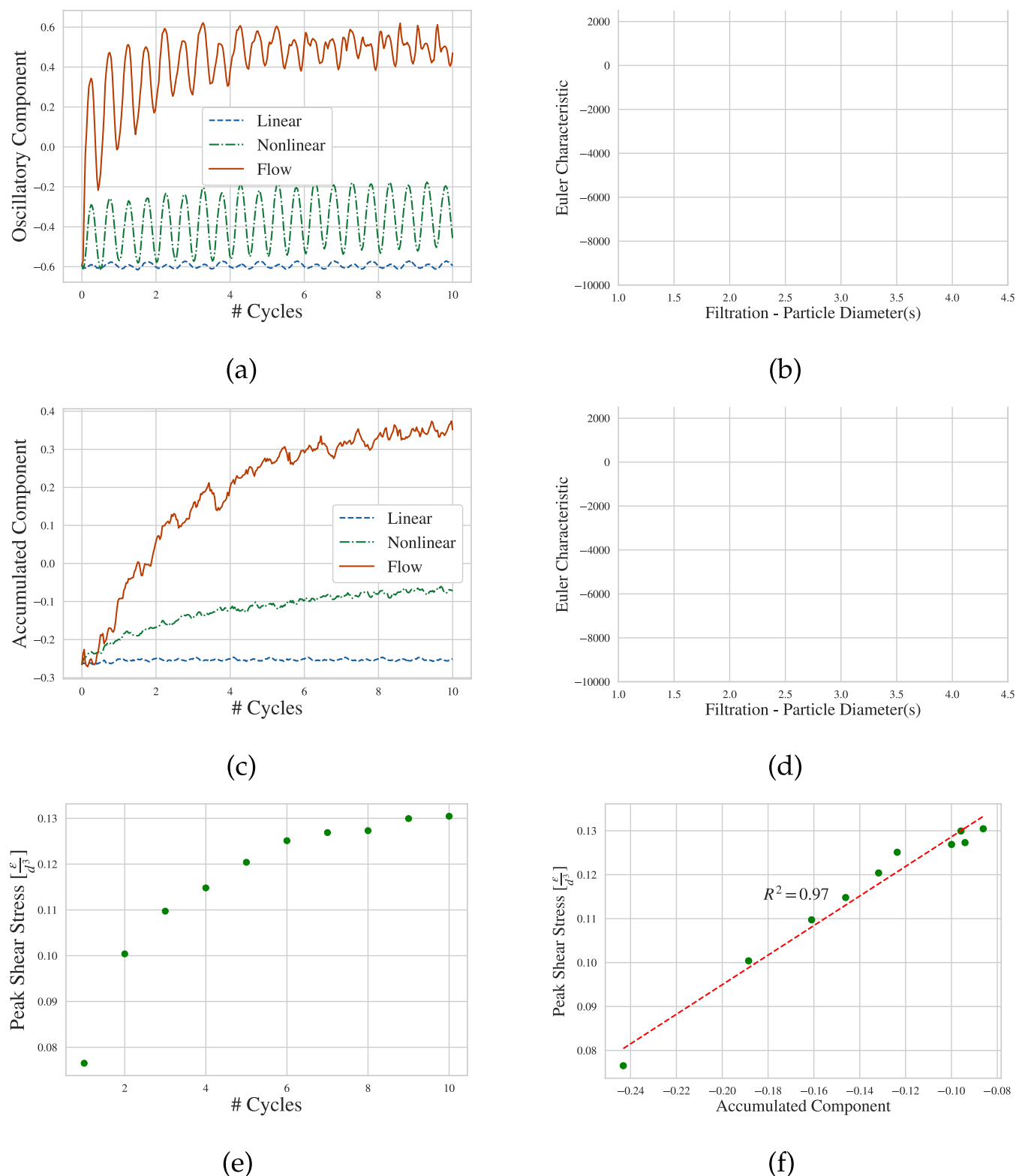
Figure 4. (a, c) Visualization of the oscillatory and cumulative component identified through PCA for gels undergoing oscillatory shear. Each component evolves over time, which illustrates the different dynamics expressed for linear, nonlinear, and flow regime responses. (b, d) Visualization of the oscillatory and cumulative component weightings for the EC curves. The area of the weightings (gray) represent higher emphasis placed on that particular portion of the EC. We see that the oscillatory component focuses on the mesoscale structure of the soft gel ($D > 2.3$ particle diameters), whereas the cumulative component focuses on the local bonding/network structure of the gel ($D < 2.3$ particle diameters). This suggests that these different scales of the material undergo different dynamics during oscillatory shear. (e, f) Demonstrates a clear correlation identified between the phenomena of shear stiffening of a gel responding nonlinearly, evidence by the increase in peak shear stress (e), and the dynamics of the cumulative component (c). We compute an $R^2 = 0.97$ which suggests that the cumulative component is an excellent predictor for the increase in peak shear stress and the phenomena of shear stiffening.
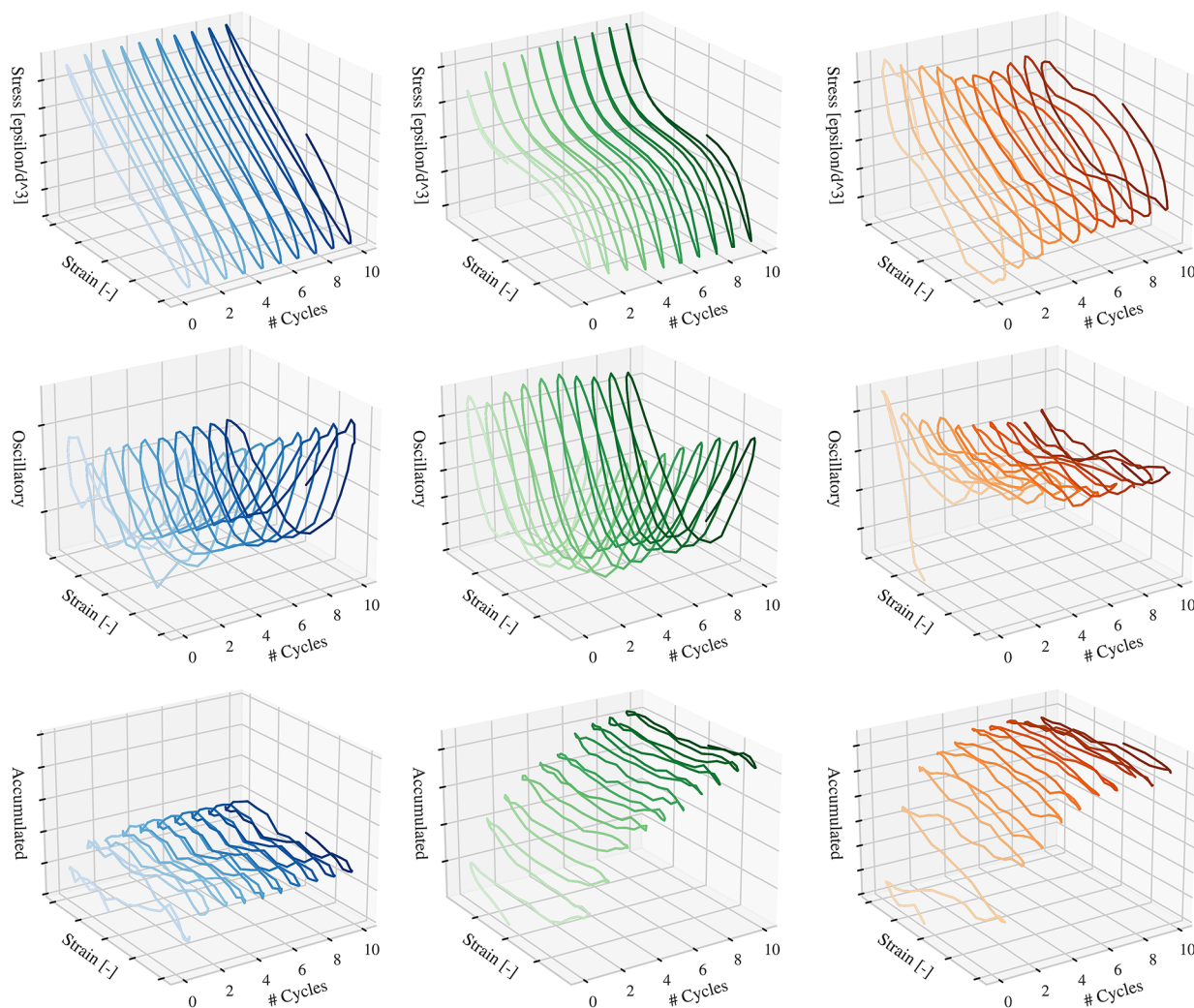
Figure 5. Comparison of the dynamics of stress, the oscillatory component, and the cumulative component versus strain in the material for the linear (left column), nonlinear (middle column), and flow (right column) regimes. We observe similar changes in oscillatory dynamics as shear amplitude increases for both stress and the oscillatory component and a dramatic change in the oscillatory component during flow that is not experienced during the linear and nonlinear shear amplitudes. We also visualize the cumulative component showing how the total cumulative damage is smoothly increased over each oscillation of the gel in the nonlinear and flow regimes, while showing minimal change in the linear regime.

regimes. First, there is a large shift in topology in the first initial oscillations of the gel, this suggests that there is immediate deformation in the mesoscale topology of the gel during flow. Furthermore, we see that as shear continues the gel reaches a new topological steady state in which the oscillations are no longer clearly defined, suggesting that there is a potential topological transition occurring at the mesoscale in the material as it undergoes flow. Physically, these changes in the EC suggest a near immediate formation of larger cavities and holes within the gel without necessarily disrupting the local bonding structure.

Moving to the cumulative component shown in Figure 4c, we see that the linear regime shows almost no change over time. The nonlinear and flow regimes show similar dynamics but with a larger magnitude change for flow. We also note there is no dramatic offset in the flow response which is seen in the oscillatory component. This dynamic mode is associated with the local network/bonding structure of the soft gel, suggesting that this cumulative structural change is capturing the breaking and forming of bonds within the soft gel, which is supported by

the weighting shown in Figure 4c. This mode is of particular interest because the structural changes are similar to those induced by reducing quench rate in gel preparation (Figure 2a), suggesting that this mode is capturing potential hardening of the gel. We explore the relationship between stiffening/hardening and the cumulative component in Figure 4e,f. Figure 4e shows the shear stress experienced by the soft gel at a shear amplitude of 0.350. This amplitude induces a nonlinear response in the gel and also stiffens the gel, this is evidenced by the increase in peak shear stress over time. Interestingly, we see a similar dynamic behavior in the cumulative component for the nonlinear response. We test whether there is a correlation between this dynamic mode and stiffening of the gel by comparing peak shear during oscillation and the corresponding value of the cumulative component at these time points, this is shown in Figure 4f. We see there is an obvious correlation between the variables ($R^2 = 0.97$), suggesting that the cumulative component could be used as a possible predictor of changes in peak shear stress. This also provides evidence that the mechanism for shear stiffening here is based on local bond reordering with minimal changes to the

mesoscopic structure of the gel, similar to what is observed when quench rates are reduced.

Combining the analysis of these components also provides insight into why this same stiffening is not observed at the amplitude corresponding to the flow transition. The cumulative component at this amplitude shows a much greater change in the local bonding structure of the gel, which would suggest a greater stiffening of the gel given the relationship found in Figure 4f for the amplitude corresponding to the maximum nonlinear elasticity. However, when comparing the oscillatory component between these amplitudes, we see minimal nonelastic deformation in the mesoscale structure of the soft gel ($D > 2$ particle diameters) in the nonlinear regime, whereas in the flow regime there is a significant reorganization of the mesoscale structure of the soft gel, which may be weakening the gel overall. Similar evidence was found in,[19] where significant bond breaking and forming was observed at high shear amplitudes (but the gel was becoming weaker). The authors hypothesized that there was a large scale reorganization of the gel, which is further supported by our topological analysis.

We can further explore the physical connections by comparing the oscillatory and cumulative dynamics identified with PCA and the stress and strain undergone by the soft gel in Figure 5. Here, we qualitatively compare the evolution of stress vs strain over each cycle and compare this to the dynamics of the oscillatory and cumulative component versus strain over each cycle. We observe strong similarities between the evolution of oscillatory component and stress when plotted against strain, illustrating similar changes in dynamics as shear amplitude increases and the dramatic change in the oscillatory component during flow that is not experienced during the linear and nonlinear shear amplitudes. This reinforces the physical connection between the topology of the soft gel and its rheological properties. We also see that the cumulative component smoothly increases over each oscillation during the nonlinear and flow regimes, while showing minimal change during the linear regime.

DISCUSSION

The structure of soft gels can be quantified effectively and efficiently through the use of topological data analysis (TDA). Specifically, we have shown that the Euler characteristic (EC) of the Čech complex of the gel network, coupled with filtration operations, captures the multiscale structure of soft gels that is missed by existing methods that focus independently on topology (e.g., bonding networks) or geometry (e.g., radial particle distributions in the physical space). We demonstrate that the EC curve provides a concise summary of the topology and geometry of soft gels and use this information to understand the physical relationships between preparation parameters (e.g., quench rate, volume fraction). Our analysis finds that there are clear continuous deformations in the structure of soft gels that correspond with changes in quench rate and volume fraction, but that the changes in the structure of the gel are not equivalent. In particular, we find that changing the quench rate impacts the local organization of the gel and that changes in the volume fraction impact both local and global structure. This suggests that fine-tuning of the quench rate and volume fraction could produce bespoke soft gels with state-of-the-art physical properties. It also indicates that applying our approach to gels formed through a range of kinetic processes can gain novel insight into the notoriously complex interplay between kinetics and gel structures.

Nonlocal constitutive behavior and microscopic dynamics of particulate gels, as well as the hierarchical nature of their viscoelastic response, have become increasingly clear. Recent studies have shown that there is a hierarchical organization of the stress transmission originating from the microscopic structure of these materials.[29] However, identifying this hierarchy directly is very challenging even in simulations, because of the complexity of the 3d disordered network structure of these materials.[18] A direct evidence of a hierarchical organization of the microstructure, apart from the cases where a clear fractal signature can be detected via scattering, has been elusive. The TDA analysis conducted in this work allowed us to clearly tease out the multiscale, hierarchical nature of the topology of the particulate gel networks. The fact that the EC changes values with varying the degree of filtration (Figures 1 and 2) quantifies precisely the different organization of the gel network over different length scales, and provides their full structural hierarchy. Figure 2 shows how this hierarchy changes as the gel is prepared through different protocols or by changing the particle volume fraction, therefore demonstrating that there is a direct link between the onset of gelation and the variation of the topological structure.

Beyond the structural analysis, we explored the dynamics of soft gels under oscillatory shear and identified significant structural changes in soft gels that occur during linear, nonlinear, and flow responses. In other words, we found that TDA tools can be used to effectively visualize dynamic effects/processes that occur to the gel structure. Specifically, our topological analysis identified a couple of dominant fast/slow dynamic modes within the sheared soft gels. These modes represent dynamics of the gel at various length scales. We show that these modes can be directly correlated to physical phenomena such as shear stiffening or hardening, and provide insight into the multiscale dynamics of complex nonlinear flow behaviors. As demonstrated in Figures 3-5, the oscillatory and cumulative components of the EC-PCA enable direct structure property relations across the entire range of amplitudes tested: more than was ever previously possible when using local microscopic observables, we can directly connect the exclusively structural information contained in the EC-PCA to the time dependent stress and strain, and therefore to the stiffening and to the macroscopic yielding of the gels.

Overall, these methods can provide significant new insight into the behavior and potential design of new soft materials that involve complex and disordered network structures. Especially, there is often the need to identify where these specific topological structures exist within a given soft gel or material. While it is not possible to map directly from the EC curve back to the soft gel, methods such as the Hodge Laplacian can be used to identify the topological structures and understand what portions of a material are contributing to their physical behavior.[62] The generalizability of the mathematical foundations for these methods makes them applicable to a wide range of data types, such as experimental images or videos. Recent advancements in 3-dimensional imaging of colloidal gels provides data that is directly amenable to the approaches proposed here and can be used to explore physical experiments, providing a route for direct comparison of particle simulation and experiments.[54−56] The approach described here can be applied directly to the experimental data in exactly the same way, to construct the simplicial complexes and the Euler characteristics, by varying the filtration radius. Experimentally, the challenges could be in reconstructing a 3d portion of the gel that is large enough, but sizes similar to those used here for the

simulations are already possible in experiments.[18,63] For the nonlinear rheological tests, an additional challenge is in following the particles during the shear deformation and flow.[64−66]

The analysis methods explored here are computationally efficient and scalable. Specifically, we are able to perform TDA computations on large simulations (in excess of 16,000 particles) in a few seconds on a single laptop computer. This is in stark contrast with other data analysis methods, such as minimum cycle basis algorithms, which scale nonlinearly in the number of particles/bonds (nodes/edges) found in a structure and only focus on a single length scale. The computational scalability make the TDA approach proposed here particularly attractive for interfacing data-mining and machine learning tools.

This work quantifies the gel structure using a data representation known as a Čech complex, but there are many other tools and methods from topology and geometry that can also be incorporated into these analyses. For example, in flocculated particle networks, the combination of topology with the Hodge Laplacian, a high-dimensional analog of the graph Laplacian for simplicial complexes, could be used to quantify the onset of and extent of flocculation, the stretch of flocks, and identify which particles are associated with dense flocks and where flocks might separate. The integration of topological concepts from knot theory, to start with, can help to understand the intertwining of soft gel structures and how the presence or absence of knots/links in the gel structure contribute to its physical characteristics.[67] The use of other methods from integral geometry, such as the full set of Minkowski functionals, can also help to understand better the full geometry of the gel structures as they undergo filtration. The Minkowski functionals (i.e., intrinsic volumes) represent orthogonal measures of intrinsic geometry and for 3-dimensional objects such as soft gels there are three independent measures: volume, surface area, and the EC.[37,68,69] Future work could therefore explore how much information those other measures can gain and how the measures connect to physical characteristics of gels such as permeability, which has been show to be directly applicable to quasi-two-dimensional materials.[70] Finally, the EC and more advanced topological characteristics such as those obtained from persistence homology, can be used to construct null-hypothesis and test for significant differences in soft gel structures.[71]

METHODS

Topological Data Analysis. Given a set of points $v \in \mathbb{R}^m$, in our case the positions of the center of mass of the particles that constitute a gel, we construct a simplicial complex built from k-simplices of varying dimension k. A k-simplex is a convex set spanned by $k + 1$ affinely independent points, denoted as

$$\sigma = \{v_1, v_2, \ldots, v_n, v_{k+1}\} \qquad (1)$$

Simplices of varying dimension are illustrated in Figure 6. A simplicial complex (denoted as $\mathcal{K}$) is obtained by connecting simplices of
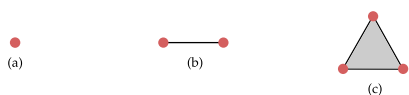

Figure 6. Examples of k-dimensional simplexes. A simplex is a generalization of a triangle to higher (or lower) dimensions. (a) 0-simplices are vertices (points), (b) 1-simplices are edges, and (c) 2-simplices are triangles.

varying dimension and can be used to describe the topology of complex shapes. In Figure 7, we use a simple 2-dimensional soft gel structure to illustrate the application of simplicial complexes to soft gel simulations. Here, the soft gel particles are represented as points in 2-dimensional space $x_i \in \mathbb{R}^2$, with a diameter $D = 1$. When a couple of particles overlap we add an edge (1-simplex) to our simplicial complex; three a triangle (2-simplex), and so on. The resulting simplicial complex is known as the nerve of the overlapping particles, and more specifically the Čech complex (see next section for more details). Simplicial complexes defined in this way are exact representations of the topology of the particle system at a given particle diameter (same number of connected component, cycles, voids, etc.) while being able to be encoded and measured using simple algebraic operations. In Figure 7a, we show how at a $D = 1$ particle diameter, many of the particles overlap with their immediate neighbors. Here, we begin to form edges or 1-dimensional simplices that begin to capture a graph structure in our data which results in four small holes and 5 different connected components, reflecting a common network representation of a soft gel. However, we can see that these holes and connected components are not randomly distributed in space, there is a larger cyclic structure that is not captured when we consider connectivity at a single particle diameter. As we move from $D = 1$ particle diameters to $D = 1.5$ particle diameters we see instances where 3 particles begin to overlap, which yields the formation of 2-dimensional simplices (e.g., filled triangles). As we continue to increase D we see increasing levels of overlap and our resulting simplicial complex is increasingly connected, revealing the larger cyclic structure captured within the Čech complex. Eventually we will reach a point where every particle is overlapped and we end up with a fully connected convex hull of our data, shown at $D = 3$ particle diameters. Through the Čech complex we gain an understanding of the geometry and topology of the soft gel at varying length scales (diameters). We note that the construction of the simplices here is similar to the application of a nearest neighbor algorithm, where nearest neighbors are defined by an increasing Euclidean distance cutoff. In some contexts it could be useful to define another method for construction of the simplicial complexes via methods such as "k"-nearest neighbors (where the number of neighbors is increased) or via an expanding neighborhood that is anisotropic around the particles to reflect nonspherical particles (e.g., liquid crystals) or to represent physical characteristics of a particular particle such as its van der Waals interaction.[72] Another common representation of structure and topology is through the Voronoi tesselation. Interestingly, the dual of the Voronoi tesselation, known as the Delaunay triangulation, can be used to construct a simplicial complex known as an Alpha complex.[73] The Alpha complex is topologically equivalent to the Čech complex at each filtration threshold and can be more memory efficient in some cases.[74]

Čech Complex. To construct a Čech complex from our soft gel particle simulations, we place at the center of each point (i.e., particle) $x_i \in \mathbb{R}^n$ an n-dimensional Euclidean ball $B(x_i, D) := \{y \in \mathbb{R}^n : \|x_i - y\|_2 < D/2\}$ of diameter $D \in \mathbb{R}$. The set of these Euclidean balls is known as a *cover* $\mathcal{U} := \cup \{B_i\}_{i \in I}$ of the points x_i, where $I \in \mathbb{Z}$ represents the total number of particles in our simulation. As we increase the diameter D of the Euclidean balls $B(x_i, D)$, we will obtain some level of overlap between balls. This overlap is what defines the connectivity, and subsequently the geometry and topology of our data. Thus, from the cover of our points $\mathcal{U}$ we obtain a shape that describes the structure of our soft gel at a length scale defined by our ball radius D (see Figure 7). From the cover of balls, we can construct a nerve which is a simplicial complex that represents exactly the topology of the overlapping balls.

The nerve of collection $\mathcal{U} := \cup \{B_{i \in I}\}$ is the simplicial complex with vertices I and k-simplices built from $\{i_0, i_1, ..., i_k\}$ if and only if $B_{i_0} \cap B_{i_1} \cap \cdots \cap B_{i_k} \neq \{\emptyset\}$. The nerve of the cover $\mathcal{U}$ is known as the Čech complex that is defined by the particle positions and selected ball diameter. We then quantify the topology of the Čech complex through the Euler characteristic.

Euler Characteristic. The Euler characteristic (EC), introduced by Leonard Euler in 1758, is a scalar value that quantifies the topological invariants of a shape. A topological invariant is a characteristic of a shape
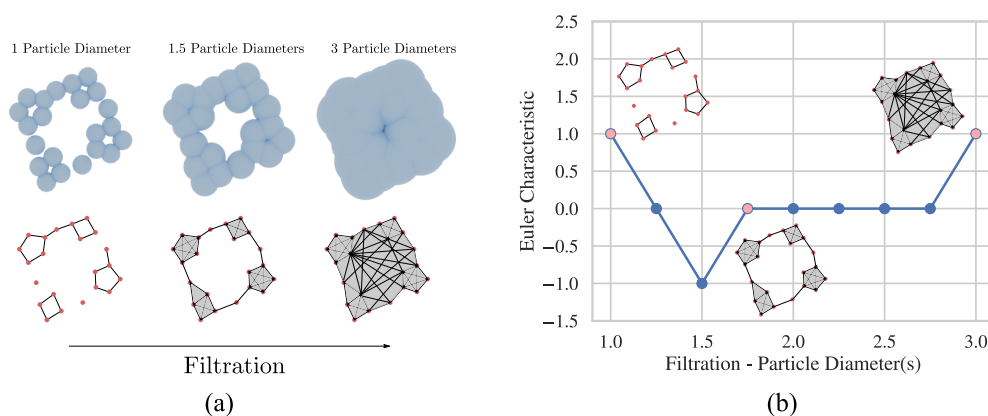
Figure 7. (a) Illustration of the changing topology of a 2-dimensional system as the diameter of the particles are increased. The overlap of the particles defines the formation of edges and higher-dimensional simplicies in the Čech complex (shown below). The Čech complex is a simplicial complex representation of the connectivity of the particles shown above. The simplicial complex representation allows us to compute and quantify the topology of the system. (b) Euler characteristic (EC) curve computed from the filtration of structure shown in (a). We measure the EC $\chi(D)$ of the Čech complex at increasing particle diameters $D_i \in \mathbb{R}$. The ordered pairing of these values $\{\chi(D_i), D_i\}$ is the EC curve. The EC curve summarizes the topological and geometrical changes in the structure at various scales.
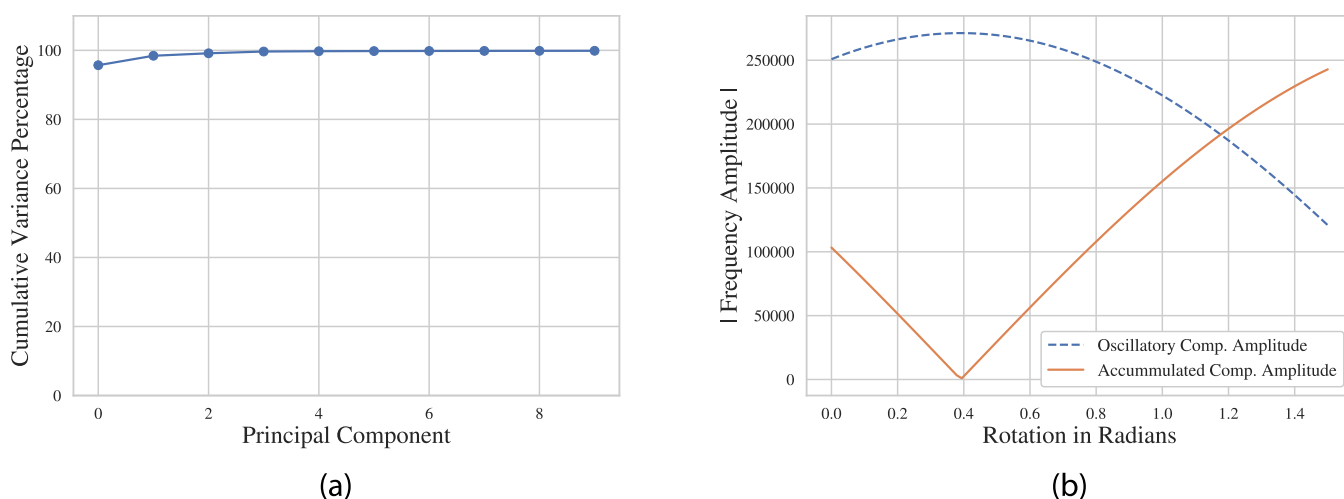

Figure 8. (a) Cumulative explained variance percentage captured with consecutive leading principal components. It is shown that the first two principal components explain over 98% of the total variance within the data set (b) illustration of the absolute amplitude of oscillation contained within the first and second component as they are rotated. We see that there is an obvious minimum amplitude in the cumulative component and maximum amplitude in the oscillatory component at a rotation of 0.40 radians which is used in our analysis.

that is unaffected by continuous deformation of the shape (e.g., stretching, bending), but is affected by discontinuous deformations (e.g., cutting, glueing). In our work, we are focused on 3-dimensional objects, which means that we are interested in three particular topological invariants: connected components (1-dimensional), holes (2-dimensional), and voids (3-dimensional). The total number of unique i-dimensional invariants in a shape are referred to as the Betti numbers β_i where i represents the dimension of the invariant being counted. The EC χ is defined as the alternating sum of the Betti numbers:

$$\chi = \sum_{i=1}^{n} (-1)^i \beta_i \tag{2}$$

Computationally, there are many ways to quantify the Betti numbers and the overall EC of a given Čech complex nerve.[48,75,76] These methods range from the use of simplicial algebra to discrete Hodge theory.[77] One of the simplest methods (we use this in our work) is an extension of Euler's original formula for polyhedra to simplicies given by[78]

$$\chi = \sum_{i=1}^{n} (-1)^i k_i \tag{3}$$

where k_i represents the number of k-dimensional simplicies in the Čech complex.

Filtration and Euler Characteristic Curves. The EC is able to effectively quantify the topology of a shape, but it does not account for all possible particle diameters and is thus sensitive to the diameter selected. We can account for this issue by applying a filtration to our data where we measure the EC at multiple, increasing particle diameters. For example, through the analysis of the simplified 2-dimensional system in Figure 7, we notice how the topology of the resulting Čech complex is sensitive to the selection of particle diameter D. This change in topology with respect to diameter provides us an understanding of the multiscale nature of the system. For example, we see that at a radius $D = 1$ particle diameters, we capture multiple small cycles in the structure, while at a larger radius $D = 1.5$ particle diameters we see that there is a much larger cycle captured. For a set of increasing diameters $D_1 < D_2 < \cdots < D_b$, we can compute the EC $\chi(D)$ of the resulting Čech complex at each diameter. From this, we can create an ordered pairing of these values to construct an Euler characteristic curve. An example curve for our simple 2-dimensional gel is found in

Figure 7. These curves summarize the evolution of the soft gel topology as we vary the diameter of the particles (moving from local to global structures). We can see in Figure 7 that we begin our filtration at $D = 1$ particle diameter which captures a series of 4 small cycles and a total of 5 connected components giving $\chi(1) = 5-1$, this structure reflects what might be analyzed in a network representation of the system. We then reach a threshold at $D = 1.5$ where we see that the smaller cycles in our graph are collapsed and we retain a single large cycle, $\chi(1.5) = 1-1$. Eventually the Cech complex becomes fully connected and we end with a single connected component at $D = 3$ particle diameters, $\chi(3) = 1-0$. We can see from Figure 7 that the EC curve quantifies and summarizes these various topological changes. Furthermore, the EC curve can be represented directly as a vector, which can be integrated into common data analysis methods such as PCA and for use in quantifying relationships between the structure of the system and its physical behavior.

Principal Component Analysis. To apply PCA we construct vectors $X_t \in \mathbb{R}^n$ of EC values $\chi(D) \in \mathbb{Z}$ of the Cech complex measured at n diameters $D \in \mathbb{R}$ for each simulation snapshot time point $t \in \mathbb{Z}$. This vector $X_t := [\chi(D_1), \chi(D_2), ..., \chi(D_n)]$ represents the EC values measured at increasing diameter $D_1 < D_2 < \cdots < D_n$. From this we can construct a matrix $\mathbb{M}$ by stacking each of our $t \in \mathbb{Z}$ simulation snapshot EC curves: $\mathbf{M} := [X_1^T, X_2^T, ... X_t^T]^T \in \mathbb{R}^{t \times n}$. We construct a matrix $\mathbf{M}_i$ for each shear amplitude $i \in 0.100, 0.350, 1.00$. In order to ensure the PCA projections are consistent across all simulations we perform PCA on all $\mathbf{M}_i$ simultaneously so that the derived principal components are the same for each simulation. Figure 3c visualizes the projection of all simulation snapshot EC curves onto the first two principal components of the collective $\mathbf{M}_i$.

The principal component analysis conducted provides an effective and interpretable dimensionality reduction for the EC curve data measured from the soft gel simulations. Here, we report the total explained variance captured in the 10 leading principal components and justify the optimal rotation of the first two principal components to separate the oscillatory and cumulative components. Figure 8a shows the cumulative variance percentage contained in the leading 10 principal components. We see that the first two components capture over 98% of the total variance in the data set supporting our selection of the first two principal components for our analysis. Figure 8b illustrates the optimal selection of rotation, in radians, for the data projected on the first two principal components in order to identify the oscillatory and cumulative components which are used in our analysis. Given data projected onto the first two principal components $\mathbf{v} = [v_1, v_2] \in \mathbb{R}^{2 \times 320}$, we apply a rotation matrix $\mathbf{R}(\theta)$ given as

$$\mathbf{R}(\theta) := \begin{bmatrix} \cos(\theta) & -\sin(\theta) \\ \sin(\theta) & \cos(\theta) \end{bmatrix}$$

where θ represents the rotation angle in radians. We can identify the optimal rotation $\hat{\theta}$ by finding the θ value that maximizes the amplitude of oscillation in the oscillatory component and minimizes the oscillatory amplitude in the cumulative component. We measure the oscillatory amplitude through a simple Fourier transform. Figure 8b shows how these two values evolve as θ is increased from 0, showing an optimal value $\hat{\theta} = 0.4$. Thus, we obtain and optimally rotated principal component projection as $\tilde{\mathbf{v}} = \mathbf{R}(0.4)\mathbf{v}$.

Numerical Gel Model and Simulation. We use an established numerical model for particulate gels[12,19,29,57,61] consisting of self-assembling spherical particles of diameter d that interact via a short-range attraction, U_2 and a three body term, U_3 which limits the bond angles and introduces a bending stiffness. This three-body term is meant to model hindrance of the relative particle motion upon aggregation, arising from sources such as particle surface roughness or irregularly shaped aggregates. The Molecular Dynamics (MD) simulations are implemented in a system of N particles with position vectors $\{\mathbf{r}_1, ..., \mathbf{r}_N\}$ and interacting with the potential energy:

$$U(\mathbf{r}_1, ..., \mathbf{r}_N) = \epsilon \left[\sum_{i > j} U_2\left(\frac{\mathbf{r}_{ij}}{d}\right) + \sum_i \sum_{j > k}^{j,k \neq i} U_3\left(\frac{\mathbf{r}_{ij}}{d}, \frac{\mathbf{r}_{ik}}{d}\right) \right] \tag{4}$$

where $\mathbf{r}_{ij} = \mathbf{r}_j - \mathbf{r}_i$, ϵ is the depth of the attractive well U_2 and sets the energy scale, and d is the particle diameter, representing the unit length scale. In typical (colloidal) systems, d corresponds approximately to the range $d \simeq 10$ to 100 nm and $\epsilon \simeq 10$ to 100 $k_B T$, where k_B is the Boltzmann constant and T, typically room temperature. The functional forms of the two-body (U_2) and three-body (U_3) terms in eq 4 are detailed elsewhere.[12,19,57,61] Gels generated with the same model and the same approach followed here have been shown to reproduce not only global behavior and rheological properties but also complex microstructural features and microscopic dynamics detected in experiments.

Gel Preparation. The preparation of the particulate gel configurations studied here has been detailed in prior works[12,30,61]; here we cover the basics of the process. The preparation protocol consists of two parts.

In a cubic simulation box of size L, we start from particles initially equilibrated at $k_B T/\epsilon = 0.5$ and brought into a spontaneously self-assembled network at $k_B T/\epsilon = 0.05$ through NVT (using a Nose-Hoover thermostat). The network is composed of strands (particles that have coordination number $z = 2$) connected by branching points ($z = 3$) and the system is further equilibrated for additional 2×10^4 MD steps.

In the second part of the gel preparation, a damped dynamics is used to bring the configuration obtained as just described to a local minimum that more likely corresponds to a mechanically stable state. This is achieved by withdrawing the kinetic energy of the system to $\sim 10^{-10}$ of its initial value with an overdamped dissipative dynamics:

$$m\frac{d^2\mathbf{r}_i}{dt^2} = -\nabla_{\mathbf{r}_i} U - \zeta\frac{d\mathbf{r}_i}{dt} \tag{5}$$

where m is the mass of each particle and ζ represents the drag coefficient due to the surrounding solvent.

For the static structural analysis detailed in Discussion, we study the effect of varying the initial quench rate between 10^{-2} and 10^{-6} $\epsilon / k_B \tau_0$ at constant volume fraction $\phi = 0.1$, and we study the effect of varying the volume fraction from 0.05 to 0.15 at a constant quench rate $\Gamma \approx 10^{-6}$ $\epsilon / k_B \tau_0$. For the rheological measurements in Methods, we exclusively study a system prepared with volume fraction $\phi = 0.1$ and quench rate $\Gamma \approx 10^{-5}$ $\epsilon / k_B \tau_0$, which has been extensively studied in prior work.[19,61]

Rheological Simulations. The rheological response is measured as in[61] by imposing an oscillatory strain signal $\gamma(t) = \gamma_0 \sin \omega t$ in the xy-plane of the simulation box through

$$m\frac{d^2\mathbf{r}_i}{dt^2} = -\nabla_{\mathbf{r}_i} U - \zeta\left(\frac{d\mathbf{r}_i}{dt} - \dot{\gamma}\left(t\right)y_i\hat{\mathbf{x}}\right) \tag{6}$$

while updating the Lees-Edwards boundary conditions at every time step. Here γ_0 is the strain amplitude and $\hat{\mathbf{x}}$ denotes the unit vector in the x-direction. In all the rheological measurements we used a Stokes-like drag with $m/\zeta = 0.5\tau_0$, having verified that the results do not change qualitatively with further decreasing the m/ζ ratio.

To systematically study how the gels' nonlinear rheological responses depend on their microstructures, we perform large amplitude oscillatory shear (LAOS) using a rate-controlled deformation:

$$\dot{\gamma}(t) = \gamma_0 \omega \cos(\omega t) \tag{7}$$

We specifically chose to perform an amplitude sweep by varying the amplitude over the range $0.001 < \gamma_0 < 10$ strain units and holding the frequency of oscillation at $\omega = 0.0025\tau_0^{-1}$. This range of strain amplitudes spans from the linear viscoelastic regime through the point where deformations are large enough to yield the material. It is worth noting that, every amplitude in this amplitude sweep corresponds to a separate rheological test that starts from the same unperturbed gel configuration.[61] This differs from most experimental amplitude sweep tests, where the different amplitudes are typically performed sequentially.

Under applied deformation, we compute the instantaneous shear stress $\sigma_{xy}(t)$. The stresses are computed from the interaction part of the global stress tensor using the standard virial equation[79] while neglecting other contributions (kinetic and viscous terms) as in previous studies.[19,61,80]

The complex viscoelastic modulus $G^*(\omega)$ is obtained from the Fourier transforms of the stress output $\sigma \sim (\omega)$ and the strain input $\gamma \sim (\omega)$ signals, as $G^*(\omega) = \sigma \sim (\omega)/\gamma \sim (\omega)$, from which we compute the storage modulus $G'(\omega)$ and the loss modulus $G''(\omega)$ defined respectively as the real and imaginary part of $G^*(\omega)$. The data used for these moduli is taken from cycles once the response has reached steady alternance[61] (typically achieved after 4−6 cycles of deformation). Prior oscillatory shear and steady shear measurements[12,19,61] indicate that the dynamic moduli are linear at small strain amplitudes (γ_0) while the response becomes nonlinear at large γ_0 values.

For three specific stress amplitudes identified from the amplitude sweep (0.1, 0.35, and 1.0 strain units) additional oscillatory tests were run for ten cycles of deformation, with rheological data and structural configurations being extracted from the system 32 times per period for use in the topological analysis discussed in Methods.

ASSOCIATED CONTENT

Data Availability Statement

All code for the topological data analysis is available via Zenodo at: 10.5281/zenodo.10909693. Raw data for particle simulations is available upon request.

AUTHOR INFORMATION

Corresponding Authors

Emanuela Del Gado − *Department of Physics, Georgetown University, Washington, DC 20057, United States; Institute for Soft Matter Synthesis and Metrology, Georgetown University, Washington DC 20057, United States;* ⊙ orcid.org/0000-0002-8340-0290; Email: ed610@georgetown.edu

Victor M. Zavala − *Department of Chemical and Biological Engineering, University of Wisconsin-Madison, Madison, Wisconsin 53706, United States; Mathematics and Computer Science Division, Argonne National Laboratory, Lemont, Illinois 60439, United States;* ⊙ orcid.org/0000-0002-5744-7378; Email: victor.zavala@wisc.edu

Authors

Alexander D. Smith − *Department of Chemical Engineering and Material Science, University of Minnesota, Minneapolis, Minnesota 55455, United States*

Gavin J. Donley − *Department of Physics, Georgetown University, Washington, DC 20057, United States*

Complete contact information is available at:
https://pubs.acs.org/10.1021/acsnano.4c04969

Notes

The authors declare no competing financial interest.
An initial draft of this manuscript can be found on the ArXiv preprint server.[81]

ACKNOWLEDGMENTS

REFERENCES

(1) Burey, P.; Bhandari, B.; Howes, T.; Gidley, M. Hydrocolloid gel particles: formation, characterization, and application. *Critical reviews in food science and nutrition* **2008**, *48*, 361−377.

(2) Tadros, T. F. *Interfacial Phenomena and Colloid Stability: Industrial Applications*; Walter de Gruyter GmbH & Co KG, 2015.

(3) Livage, d. J.; Lemerle, J. Transition metal oxide gels and colloids. *Annu. Rev. Mater. Sci.* **1982**, *12*, 103−122.

(4) Cao, Y.; Mezzenga, R. Design principles of food gels. *Nature Food* **2020**, *1*, 106−118.

(5) Dickinson, E. Microgels—An alternative colloidal ingredient for stabilization of food emulsions. *Trends in Food Science & Technology* **2015**, *43*, 178−188.

(6) Townsend, J. M.; Beck, E. C.; Gehrke, S. H.; Berkland, C. J.; Detamore, M. S. Flow behavior prior to crosslinking: The need for precursor rheology for placement of hydrogels in medical applications and for 3D bioprinting. *Prog. Polym. Sci.* **2019**, *91*, 126−140.

(7) Wang, H.; Boerman, O. C.; Sariibrahimoglu, K.; Li, Y.; Jansen, J. A.; Leeuwenburgh, S. C. Comparison of micro-vs. nanostructured colloidal gelatin gels for sustained delivery of osteogenic proteins: Bone morphogenetic protein-2 and alkaline phosphatase. *Biomaterials* **2012**, *33*, 8695−8703.

(8) Zhang, H. *Building materials in civil engineering*; Elsevier, 2011.

(9) Yan, L.; Kasal, B.; Huang, L. A review of recent research on the use of cellulosic fibres, their fibre fabric reinforced cementitious, geo-polymer and polymer composites in civil engineering. *Composites Part B: Engineering* **2016**, *92*, 94−132.

(10) Ioannidou, K.; Krakowiak, K. J.; Bauchy, M.; Hoover, C. G.; Masoero, E.; Yip, S.; Ulm, F.-J.; Levitz, P.; Pellenq, R. J.-M.; Del Gado, E. Mesoscale texture of cement hydrates. *Proc. Natl. Acad. Sci. U. S. A.* **2016**, *113*, 2029−2034.

(11) Liu, R.; Sun, Z.; Ding, Q.; Chen, P.; Chen, K. Mitigation of early-age cracking of concrete based on a new gel-type superabsorbent polymer. *J. Mater. Civil Eng.* **2017**, *29*, No. 04017151.

(12) Bouzid, M.; Del Gado, E. Network topology in soft gels: Hardening and softening materials. *Langmuir* **2018**, *34*, 773−781.

(13) Bouzid, M.; Del Gado, E. Mechanics of soft gels: Linear and nonlinear response. *Handbook of Materials Modeling: Applications: Current and Emerging Materials* **2020**, 1719−1746.

(14) Lieleg, O.; Kayser, J.; Brambilla, G.; Cipelletti, L.; Bausch, A. R. Slow dynamics and internal stress relaxation in bundled cytoskeletal networks. *Nature materials* **2011**, *10*, 236−242.

(15) Conrad, J.; Wyss, H.; Trappe, V.; Manley, S.; Miyazaki, K.; Kaufman, L.; Schofield, A. B.; Reichman, D.; Weitz, D. Arrested fluid-fluid phase separation in depletion systems: Implications of the characteristic length on gel formation and rheology. *J. Rheol.* **2010**, *54*, 421−438.

(16) Koumakis, N.; Moghimi, E.; Besseling, R.; Poon, W. C.; Brady, J. F.; Petekidis, G. Tuning colloidal gels by shear. *Soft Matter* **2015**, *11*, 4640−4648.

(17) Burla, F.; Dussi, S.; Martinez-Torres, C.; Tauber, J.; van der Gucht, J.; Koenderink, G. H. Connectivity and plasticity determine collagen network fracture. *Proc. Natl. Acad. Sci. U. S. A.* **2020**, *117*, 8326−8334.

(18) Nabizadeh, M.; Nasirian, F.; Li, X.; Saraswat, Y.; Waheibi, R.; Hsiao, L. C.; Bi, D.; Ravandi, B.; Jamali, S. Network physics of attractive colloidal gels: Resilience, rigidity, and phase diagram. *Proc. Natl. Acad. Sci. U. S. A.* **2024**, *121*, No. e2316394121.

(19) Colombo, J.; Del Gado, E. Stress localization, stiffening, and yielding in a model colloidal gel. *J. Rheol.* **2014**, *58*, 1089−1116.

(20) Manley, S.; Davidovitch, B.; Davies, N. R.; Cipelletti, L.; Bailey, A.; Christianson, R. J.; Gasser, U.; Prasad, V.; Segre, P.; Doherty, M.; et al. Time-dependent strength of colloidal gels. *Physical review letters* **2005**, *95*, No. 048302.

(21) Sudreau, I.; Servel, M.; Freyssingeas, E.; Liénard, F. m. c.; Karpati, S.; Parola, S.; Jaurand, X.; Dugas, P.-Y.; Matthews, L.; Gibaud, T.;

Divoux, T.; Manneville, S. Shear-induced stiffening in boehmite gels: A rheo-X-ray-scattering study. *Phys. Rev. Mater.* **2023**, *7*, No. 115603.

(22) Moghimi, E.; Jacob, A. R.; Koumakis, N.; Petekidis, G. Colloidal gels tuned by oscillatory shear. *Soft Matter* **2017**, *13*, 2371−2383.

(23) Gibaud, T.; Dagès, N.; Lidon, P.; Jung, G.; Ahouré, L. C.; Sztucki, M.; Poulesquen, A.; Hengl, N.; Pignon, F.; Manneville, S. Rheoacoustic gels: tuning mechanical and flow properties of colloidal gels with ultrasonic vibrations. *Physical Review X* **2020**, *10*, No. 011028.

(24) Bonn, D.; Denn, M. M.; Berthier, L.; Divoux, T.; Manneville, S. Yield stress materials in soft condensed matter. *Rev. Mod. Phys.* **2017**, *89*, No. 035005.

(25) Israelachvili, J. *Intermolecular and Surface Forces*, 3rd ed.; Academic Press, 2011.

(26) Dinsmore, A. D.; Prasad, V.; Wong, I. Y.; Weitz, D. A. Microscopic Structure and Elasticity of Weakly Aggregated Colloidal Gels. *Phys. Rev. Lett.* **2006**, *96*, No. 185502.

(27) Whitaker, K. A.; Varga, Z.; Hsiao, L. C.; Solomon, M. J.; Swan, J. W.; Furst, E. M. Colloidal gel elasticity arises from the packing of locally glassy clusters. *Nat. Commun.* **2019**, *10*, 2237.

(28) Royall, C. P.; Faers, M. A.; Fussell, S. L.; Hallett, J. E. Real space analysis of colloidal gels: triumphs, challenges and future directions. *J. Phys.: Condens. Matter* **2021**, *33*, No. 453002.

(29) Bantawa, M.; Keshavarz, B.; Geri, M.; Bouzid, M.; Divoux, T.; McKinley, G.; Del Gado, E. The hidden hierarchical nature of soft particulate gels. *Nat. Phys.* **2023**, *19*, 1178−1184.

(30) Bouzid, M.; Colombo, J.; Barbosa, L. V.; Del Gado, E. Elastically driven intermittent microscopic dynamics in soft solids. *Nat. Commun.* **2017**, *8*, No. 15846.

(31) Aime, S.; Ramos, L.; Cipelletti, L. Microscopic dynamics and failure precursors of a gel under mechanical load. *Proc. Natl. Acad. Sci. U. S. A.* **2018**, *115*, 3587−3592.

(32) Keshavarz, B.; Rodrigues, D. G.; Champenois, J.-B.; Frith, M. G.; Ilavsky, J.; Geri, M.; Divoux, T.; McKinley, G. H.; Poulesquen, A. Time−connectivity superposition and the gel/glass duality of weak colloidal gels. *Proc. Nat. Acad. Sci.* **2021**, *118*, No. e2022339118.

(33) Hsiao, L. C.; Newman, R. S.; Glotzer, S. C.; Solomon, M. J. Role of isostaticity and load-bearing microstructure in the elasticity of yielded colloidal gels. *Proc. Natl. Acad. Sci. U. S. A.* **2012**, *109*, 16029−16034.

(34) Ohtsuka, T.; Royall, C. P.; Tanaka, H. Local structure and dynamics in colloidal fluids and gels. *Europhys. Lett.* **2008**, *84*, 46002.

(35) Varadan, P.; Solomon, M. J. Direct visualization of long-range heterogeneous structure in dense colloidal gels. *Langmuir* **2003**, *19*, 509−512.

(36) Smith, A.; Zavala, V. M. The Euler characteristic: A general topological descriptor for complex data. *Comput. Chem. Eng.* **2021**, *154*, No. 107463.

(37) Mantz, H.; Jacobs, K.; Mecke, K. Utilizing Minkowski functionals for image analysis: a marching square algorithm. *Journal of Statistical Mechanics: Theory and Experiment* **2008**, *2008*, No. P12015.

(38) Jiao, Y.; Stillinger, F.; Torquato, S. Modeling heterogeneous materials via two-point correlation functions: Basic principles. *Phys. Rev. E* **2007**, *76*, No. 031110.

(39) Arizzi, S.; Mott, P.; Suter, U. Space available to small diffusants in polymeric glasses: analysis of unoccupied space and its connectivity. *J. Polym. Sci., Part B: Polym. Phys.* **1992**, *30*, 415−426.

(40) Hansen, P. H.; Rödner, S.; Bergström, L. Structural characterization of dense colloidal films using a modified pair distribution function and Delaunay triangulation. *Langmuir* **2001**, *17*, 4867−4875.

(41) Lotito, V.; Zambelli, T. Pattern detection in colloidal assembly: A mosaic of analysis techniques. *Advances in colloid and interface science* **2020**, *284*, No. 102252.

(42) Karnes, J. J.; Weisgraber, T. H.; Oakdale, J. S.; Mettry, M.; Shusteff, M.; Biener, J. On the network topology of cross-linked acrylate photopolymers: a molecular dynamics case study. *J. Phys. Chem. B* **2020**, *124*, 9204−9215.

(43) Glielmo, A.; Husic, B. E.; Rodriguez, A.; Clementi, C.; Noé, F.; Laio, A. Unsupervised learning methods for molecular simulation data. *Chem. Rev.* **2021**, *121*, 9722−9758.

(44) Kaveh, A.; Roosta, G. Revised Greedy algorithm for formation of a minimal cycle basis of a graph. *Communications in numerical methods in engineering* **1994**, *10*, 523−530.

(45) Smith, A.; Runde, S.; Chew, A.; Kelkar, A.; Maheshwari, U.; Van Lehn, R.; Zavala, V. Topological Analysis of Molecular Dynamics Simulations using the Euler Characteristic. *J. Chem. Theory Comput.* **2023**, *19*, 1553.

(46) Rocks, J. W.; Liu, A. J.; Katifori, E. Hidden topological structure of flow network functionality. *Phys. Rev. Lett.* **2021**, *126*, No. 028102.

(47) Rocks, J. W.; Liu, A. J.; Katifori, E. Revealing structure-function relationships in functional flow networks via persistent homology. *Physical Review Research* **2020**, *2*, No. 033234.

(48) Smith, A. D.; Dłotko, P.; Zavala, V. M. Topological data analysis: concepts, computation, and applications in chemical engineering. *Comput. Chem. Eng.* **2021**, *146*, No. 107202.

(49) Chung, M. K.; Smith, A.; Shiu, G. Reviews: Topological distances and losses for brain networks *arXiv* 2021. Preprint arXiv:2102.08623.

(50) Obayashi, I.; Nakamura, T.; Hiraoka, Y. Persistent homology analysis for materials research and persistent homology software: HomCloud. *J. Phys. Soc. Jpn.* **2022**, *91*, No. 091013.

(51) Nakamura, T.; Hiraoka, Y.; Hirata, A.; Escolar, E. G.; Nishiura, Y. Persistent homology and many-body atomic structure for medium-range order in the glass. *Nanotechnology* **2015**, *26*, No. 304001.

(52) Mecke, K.; Wagner, H. Euler characteristic and related measures for random geometric sets. *J. Stat. Phys.* **1991**, *64*, 843−850.

(53) Klee, V. The Euler characteristic in combinatorial geometry. *American Mathematical Monthly* **1963**, *70*, 119−127.

(54) Dinsmore, A.; Weitz, D. Direct imaging of three-dimensional structure and topology of colloidal gels. *J. Phys.: Condens. Matter* **2002**, *14*, 7581.

(55) Dong, J.; Turci, F.; Jack, R. L.; Faers, M. A.; Royall, C. P. Direct imaging of contacts and forces in colloidal gels. *J. Chem. Phys.* **2022**, *156*, No. 214907.

(56) Habdas, P.; Weeks, E. R. Video microscopy of colloidal suspensions and colloidal crystals. *Curr. Opin. Colloid Interface Sci.* **2002**, *7*, 196−203.

(57) Bantawa, M.; Fontaine-Seiler, W. A.; Olmsted, P. D.; Del Gado, E. Microscopic interactions and emerging elasticity in model soft particulate gels. *J. Phys.: Condens. Matter* **2021**, *33*, No. 414001.

(58) Dibble, C. J.; Kogan, M.; Solomon, M. J. Structural origins of dynamical heterogeneity in colloidal gels. *Phys. Rev. E* **2008**, *77*, No. 050401(R).

(59) Horton, J. D. A polynomial-time algorithm to find the shortest cycle basis of a graph. *SIAM Journal on Computing* **1987**, *16*, 358−366.

(60) Ruiz-Franco, J.; Gnan, N.; Zaccarelli, E. Rheological investigation of gels formed by competing interactions: A numerical study. *J. Chem. Phys.* **2019**, *150*, No. 024905.

(61) Donley, G. J.; Bantawa, M.; Del Gado, E. Time-resolved microstructural changes in large amplitude oscillatory shear of model single and double component soft gels. *J. Rheol.* **2022**, *66*, 1287−1304.

(62) Wei, R. K. J.; Wee, J.; Laurent, V. E.; Xia, K. Hodge theory-based biomolecular data analysis. *Sci. Rep.* **2022**, *12*, 9699.

(63) Müller, F.; Isa, L.; Vermant, J. Toughening colloidal gels using rough building blocks. *Nat. Commun.* **2023**, *14*, 5309.

(64) Vasisht, V. V.; Dutta, S. K.; Del Gado, E.; Blair, D. L. Rate Dependence of Elementary Rearrangements and Spatiotemporal Correlations in the 3D Flow of Soft Solids. *Phys. Rev. Lett.* **2018**, *120*, No. 018001.

(65) Jiang, Y.; Makino, S.; Royer, J. R.; Poon, W. C. K. Flow-Switched Bistability in a Colloidal Gel with Non-Brownian Grains. *Phys. Rev. Lett.* **2022**, *128*, No. 248002.

(66) Edera, P.; Brizioli, M.; Madani, M.; Ngouamba, E.; Coussot, P.; Trappe, V.; Petekidis, G.; Giavazzi, F.; Cerbino, R.Yielding under the microscope: a multi-scale perspective on brittle and ductile behaviors in oscillatory shear. *Soft Condens. Matter* **2024**, https://arxiv.org/abs/2402.00221

(67) Horner, K. E.; Miller, M. A.; Steed, J. W.; Sutcliffe, P. M. Knot theory in modern chemistry. *Chem. Soc. Rev.* **2016**, *45*, 6432−6448.

(68) Hütter, M. Heterogeneity of colloidal particle networks analyzed by means of Minkowski functionals. *Phys. Rev. E* **2003**, *68*, No. 031404.

(69) Koehl, P.; Akopyan, A.; Edelsbrunner, H. Computing the Volume, Surface Area, Mean, and Gaussian Curvatures of Molecules and Their Derivatives. *J. Chem. Inf. Model.* **2023**, *63*, 973−985.

(70) Scholz, C.; Wirner, F.; Götz, J.; Rüde, U.; Schröder-Turk, G. E.; Mecke, K.; Bechinger, C. Permeability of porous materials determined from the Euler characteristic. *Physical review letters* **2012**, *109*, No. 264504.

(71) Dłotko, P.; Hellmer, N.; Stettner, Ł.; Topolnicki, R. Topology-driven goodness-of-fit tests in arbitrary dimensions. *Stat. Comput.* **2024**, *34*, 34.

(72) Myers, A.; Munch, E.; Khasawneh, F. A. Persistent homology of complex networks for dynamic state detection. *Phys. Rev. E* **2019**, *100*, No. 022314.

(73) MacPherson, R.; Schweinhart, B. Measuring shape with topology. *J. Math. Phys.* **2012**, *53*, No. 073516.

(74) Edelsbrunner, H.; Morozov, D. *Handbook of Discrete and Computational Geometry*; Chapman and Hall/CRC, 2017; pp 637−661.

(75) Edelsbrunner, H.; Harer, J.; et al. Persistent homology-a survey. *Contemporary mathematics* **2008**, *453*, 257−282.

(76) Edelsbrunner, H.; Harer, J. L. *Computational topology: an introduction*; American Mathematical Society, 2022.

(77) Knill, O.One can hear the Euler characteristic of a simplicial complex. *arXiv* 2017. Preprint arXiv:1711.09527.

(78) Richeson, D. S. *Euler's gem: the polyhedron formula and the birth of topology*; Princeton University Press, 2019.

(79) Thompson, A.; Plimpton, S.; Mattson, W. General formulation of pressure and stress tensor for arbitrary many-body interaction potentials under periodic boundary conditions. *J. Chem. Phys.* **2009**, *131*, No. 154107.

(80) Bouzid, M.; Gado, E. D. *Handbook of Materials Modeling: Applications: Current and Emerging Materials; Springer International Publishing: Cham* **2018**, 1−29.

(81) Smith, A.; Donley, G. J.; Del Gado, E.; Zavala, V. M.Topological Data Analysis for Particulate Gels. *arXiv* **2024**. Preprint arXiv:2404.02991 2024 (accessed August, 2024).